# Modelling of mass transport and insulin secretion of a membrane-based encapsulation device of pancreatic islets

## Katarzyna Skrzypek[a], Efrem Curcio[b,*], Dimitrios Stamatialis[a]

[a] (Bio)artificial Organs, TechMed Institute of Biomedical Technology and Technical Medicine, Faculty of Science and Technology, University of Twente, 7500AE, Enschede, The Netherlands
[b] Department of Environmental and Chemical Engineering, University of Calabria. Via P. Bucci CUBO 45A, 87036 Rende, CS, Italy

## ARTICLE INFO

## ABSTRACT

Widespread application of islet transplantation as a cure for type 1 Diabetes Mellitus patients is limited mainly due to the need for life-long immunosuppression associated with serious side effects. Immunoisolation by encapsulation of islets in semi-permeable membranes may overcome this issue as it allows for transplantation potentially obviating the need for immunosuppressive drug therapy.

This work focuses on the development and validation of a model of the mass transfer and secretion kinetics of insulin – the major regulator of glucose homeostasis – in a new microwell membrane based encapsulation device for pancreatic islets. Due to the high number and complexity of parameters that determine the effectiveness of the device, the implementation of a reliable numerical model is of critical importance for optimization of the micro-confined bioengineered environment. The simultaneous solution of mass transfer and uptake/production reactions occurring through the polymeric membrane system and within the islets allows detailed description of the spatial distribution profiles of insulin, glucose, and oxygen with the aim to assure an adequate insulin dynamics. The simulation tool, experimentally validated, is used to improve the scaffold geometry with the aim to assure adequate responsiveness and function over time for future clinical implementation of the device.

## 1. Introduction

In healthy human subjects, preservation of blood glucose levels within the range of 3.5–7.0 mM occurs from a finely tuned glucose-insulin control system mediated by β-cells (Daly et al., 1998). These cells are located in pancreatic islets (or "islets of Langerhans"), spheroidal aggregates of hormone-secreting endocrine cells of different types (α, β, γ and PP-cells) with typical diameters of $100-150\,\mu m$ (Buchwald et al., 2009). Failure in β-cell function is the basis of type 1 (insulin-dependent or juvenile-onset) diabetes, a pervasive autoimmune disease.

The effectiveness of pancreatic islet transplantation via direct infusion into the liver, attempted as alternative to insulin therapy and to occurrence of hyper- and hypo-glycemic events (Shapiro et al., 2017), is generally limited by a high degree of islet loss in the immediate post-transplant period (Emamaullee and Shapiro, 2006) and requires use of life-long immunosuppression. The necessity to maintain functionality and to provide immune protection of transplanted pancreatic islets has driven researchers towards the development of bioengineered encapsulation devices based on a large variety of encapsulation biomaterials such as, alginate (Strand et al., 2017), polyethylene glycol, polylactide derived (de Vos et al., 2014; Liao et al., 2013) etc. Current encapsulation approaches, although preserving islet function, fail in providing long-term islet survival due to mass transfer limitation of encapsulation system in terms of the diffusion of nutrients and wastes. Development of 3-dimensional scaffolds (i.e. poly(lactide-co-glycolide) (PLGA)

---

matrices with interconnected pores (Borg and Bonifacio, 2011), polyglycolic acid fibrous scaffold (Chun et al., 2008) etc.) allows for cell seeding into pores with easy access to necessary nutrients. However, cell encapsulation using scaffolds with suboptimal pore size my cause tissue in-growth and host cell penetration, making necessary the use of immunosuppressive drugs.

Membranes, with their intrinsic characteristics of high selectivity at molecular level and permeability for the transport of specific components, allow transport of nutrients to cells while providing an efficient removal of catabolites and metabolic products. Moreover, availability of membranes in a wide spectrum of molecular weight cut-off (MWCO) makes them effective immunoisolation barriers to immunocompetent species without need for immunosuppression therapy (Lien et al., 2019; Curcio et al., 2012). In earlier studies, we have developed a membrane based macroencapsulation system where the pancreatic islets are confined between microwell membranes to allow bidirectional diffusion of nutrients and catabolites, to immune-isolate cells and protect them from mechanical stress, and to prevent clustering of islets and consequent cell death due to mass transport hindrance in large aggregates (Skrzypek et al., 2017, 2018a; Skrzypek et al., 2018b; Groot Nibbelink et al., 2018). This microwell device, prepared using porous membranes based on polymer blend of Polyethersulfone/Polyvinyl pyrrolidone (PES/PVP), has good biocompatibility and prevascularization potential in vivo (Skrzypek et al., 2018b) and shows very promising results related to insulin delivery in vitro (Skrzypek et al., 2017, 2018a). However, the device is rather large for implantation to humans and, therefore, optimization of microwell membrane dimensions (microwell size, spacing etc.) is required.

In this work, first a theoretical model is developed and computationally implemented focusing on the detailed spatial distribution of oxygen gradient and insulin secretion within the device: a Finite Element Method (FEM) is adopted to predict combined diffusive mass transport with uptake/production rate of insulin, glucose and oxygen. The model is validated using experimental results and then implemented to design an improved microwell device with optimal characteristics for clinical application.

## 2. Materials and methods

### 2.1. MIN6 and human pancreatic islets

For the development and validation of model, experimental data sets were used from (Skrzypek et al., 2017). Briefly, these investigations were carried out using mouse insulinoma MIN6-B1 cell aggregates, and human islets of Langerhans. The protocols for mouse insulinoma cell culture and consequent pseudo-islets formation are detailed in Skrzypek et al. (2017). MIN6-B1 cells were cultured in Dulbecco's Modified Eagle's Medium (DMEM, Gibco) supplemented with 10% (v/v) FBS (Lonza), 100 U/mL penicillin and 100 mg/mL streptomycin (Gibco), and 70 μM freshly added beta-mercaptoethanol (Gibco) at 37 °C and 5% CO$_2$. For the formation of stable cellular aggregates, MIN6 cells (~250 cells per pseudo-islet) were seeded onto sterile agarose chips fabricated according to methodology elucidated in Rivron et al. (2012). Chips were centrifuged at 150 g for 1 min, and carefully subjected to addition of 2 mL of medium. After two days at 37 °C, stable spheroids were flushed out of the chips and used in microwell membrane systems.

Human islets of Langerhans (isolated from 3 donor pancreata and provided by the Leiden University Medical Center, The Netherlands) were used in compliance with national regulations. Islets were cultured in CMRL 1066 medium (5.5 mmol/L glucose) containing 10% FBS, 2 mM GlutaMAX, 100 mU/mL penicillin and 1 mg/mL streptomycin (Gibco), 10 mmol/L HEPES, and 1.2 mg/mL nicotinamide.

### 2.2. Microwell membrane system fabrication

The microwell membrane was fabricated by phase separation micro-molding (PSμM) (Papenburg et al., 2007). A polymeric solution, composed by 15 wt.% polyethersulfone (PES) (Ultrason, E6020 P), 5 wt.% polyvinylpyrrolidone (PVP) (MW = 40000,Sigma Aldrich) and N-methylpyrrolidone (NMP) (Acros organic), was stirred overnight at room temperature and, then, cast on a silicon micropatterned mold to obtain a bi-dimensional array of microwells with diameter and depth of 430 μm and 330 μm, respectively (Fig. 1). Two microwell membranes were fabricated having membrane thickness of 250 and 100 μm, respectively. The transwell membrane system was treated with 4000 ppm sodium hypochlorite aqueous solution (NaClO, Fluka) to increase its porosity.

The performance of the closed encapsulation device was investigated by covering the microwell membrane with a porous flat PES membrane, as a lid, with thickness of 150 μm and pore size of 0.45 μm (Fig. 1f–g). The lid was used with the aim to protect the islets from immune cells, while permitting nutrient inflow and metabolite outflow. The microwell membrane device without lid is indicated as "open system"; this configuration was adopted in order to investigate insulin secretion having a lower impact of mass transfer resistances on reaction kinetics. Sterilization was carried out using 70% ethanol for 30 min and washed 3 times in phosphate-buffered saline (PBS).

### 2.3. Mathematical modeling and simulation

Fig. 1 presents top view and cross-section of the Scanning Electron Microscopy (SEM) images of the encapsulation device that served as reference for the computational modeling of the. A 2D model of the longitudinal cross-section for a portion of the device – i.e. five adjacent microwells – has been implemented. A single microwell acts as an insulated subsystem, and the corresponding rotational symmetry axis that intersects the center of each microwell defines the spherical shape of the cellular aggregate and the cylindrical form of the well, coherently with the real spatial geometry of the system. Each microwell contains a single cultured spherical islet or MIN6 aggregate of diameter of 150 μm.

Simultaneous diffusion and reaction of oxygen, glucose and insulin was described by the following parabolic partial differential equation (PDE) expressed in 2-D space:

$$\frac{\partial c_i}{\partial t} = D_i(x, y) \left( \frac{\partial^2 c_i}{\partial x^2} + \frac{\partial^2 c_i}{\partial y^2} \right) \pm r_i \tag{1}$$

where c is the molar concentration of the species (mol/cm$^3$), t is the time (s), $D_i$ is the diffusion coefficient of the i-th species (cm$^2$/s), and $r_i$ the reaction rate (negative for oxygen and glucose uptake and positive for insulin secretion) expressed in mol/(cm$^3$s). Eq. (1) was derived from mass conservation principles, assuming diffusive transport only (no convective flow was adopted in experimental tests) and zero-order oxygen and glucose consumption according to previous studies (Papenburg et al., 2011).

For the insulin secretion rate (further details in Supporting information), a two-phases kinetic model was considered, combining a first-order response function with an exponentially decreasing time-function (Thrash, 2010; Buladi et al.,
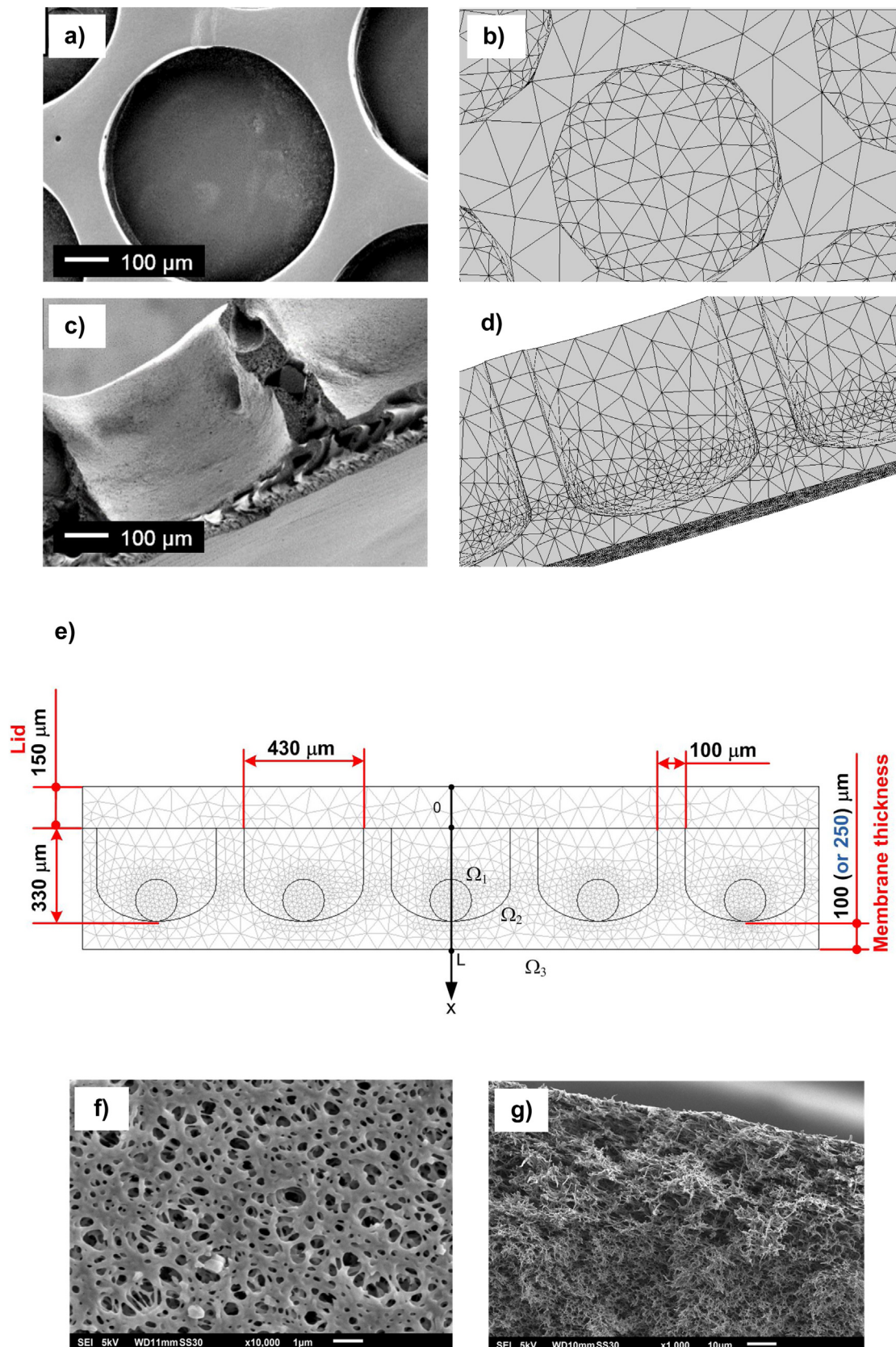
Fig. 1 – Microwell membrane system for pancreatic islet encapsulation: (a) top-view SEM micrograph; (b) top-view of the simulated system meshed into triangular elements; (c) cross-sectional SEM micrograph; (d) cross-section of the simulated system; (e) 2D cross-sectional view of the simulated portion of the closed system, i.e. 5 adjacent microwells with 150 μm MIN6 aggregate in each well and 100 μm membrane thickness (investigations have been also carried out on 250 μm membrane thickness). Here the porous lid is closing the transwell membrane system; (f) top-view SEM micrograph; (g) cross-sectional SEM micrograph.

1996). Phase I includes a linear increase in production rate until a characteristic time $t_I^*$:

$$r_I(t \leq t_1^*) = \beta \cdot t \tag{2.a}$$

where $\beta$ is a constant, in mol/(cm$^3$s$^2$).

The successive Phase II is characterized by an explicit dependence of insulin secretion rate on the glucose concentration ($c_G$):

$$r_I(t > t_1^*) = Ae^{-\alpha_1(t-t_1^*)} + B\left[1 - e^{-\alpha_2(t-t_2^*)}\right] \tag{2.b}$$

where:

$$A = \frac{V_{m,1}(c_G - c_{G,1})}{K_{m,1} + (c_G - c_{G,1})} \tag{2.c}$$

$$B = \frac{V_{m,2}(c_G - c_{G,2})}{K_{m,2} + (c_G - c_{G,2})} \tag{2.d}$$

Kinetic parameters and diffusional rates are listed in Table 1. In Eqs. (2.a)–(2.d) parameters $K_{m1}$, $K_{m2}$, $c_{G,1}$ and $c_{G,2}$ have been deduced from literature (Thrash, 2010), while other parameters have been adjusted in order to fit experimental insulin secretion data reported in Section 3.1. The model is implemented and solved in three compartments: cell culture medium, islet and the microwell encapsulation system.

For the i-th component (O$_2$: oxygen, G: glucose, I: insulin), Eq. (1) is solved for the following initial conditions:

$$t = 0, c_i = c_i^0 \tag{3.a}$$

where values for $c_i^0$ are provided in Table 1. Specifically, the initial condition for oxygen corresponds to the O$_2$ concentration dissolved in the medium equilibrated with a 20% O$_2$ partial pressure. For glucose, an initial concentration in CMRL 1066 culture medium (5.5 mM) is considered, except for the case of glucose-induced insulin secretion test (Section 2.4) where initial step concentration values are, alternatively, 1.67 mM (Low Glucose Concentration, LGC) and 16.7 mM (High Glucose Concentration, HGC). The initial insulin concentration is zero.

Additionally, the following boundary conditions are assumed:

$$x = 0, c_{O_2} = H \cdot p_{O_2}, c_G = c_G^{medium,TOP} \begin{cases} LGC : 1.67 \, mM \\ HGC : 16.7 \, mM \end{cases} \tag{3.b}$$

expressing the equilibrium condition for oxygen at the gas-liquid interface as described according to the Henry law, with H = $9.97 \times 10^{-4}$ mol/(L atm) for aqueous media (Curcio et al., 2014), and the condition for glucose concentration equal to LGC or HGC;

$$x = \Omega_1, \Omega_2, \Omega_3 \left. \frac{\partial c_i}{\partial x} \right|_{x=\Omega_i} = 0 \tag{3.c}$$

expressing the continuity at the interface medium-islet and medium-wall side of the wells, symmetry at the edges of the scaffold;

$$x = L, c_{O_2} = H \cdot p_{O_2}, c_G = c_G^{medium,BOTTOM} \begin{cases} LGC : 1.67 \, mM \\ HGC : 16.7 \, mM \end{cases} \tag{3.d}$$

with analogous meaning of boundary condition (3.b).

For the case of a transwell membrane system covered by the lid ("closed system"), the boundary condition (3.b) is localized at the top of the lid, while Eq. (3.c) is applied also to describe the continuity at the interface lid-medium and lid-wall side of the wells.

The set of PDEs, written in Cartesian coordinate system, was numerically integrated by COMSOL MULTIPHYSICS v4.2 – Chemical engineering module using finite element method (FEM). The modelled system was meshed into 3400 triangular elements and solved and as time-dependent problem with relative tolerance of $10^{-6}$ for 20,682 degrees of freedom. Computer simulation was carried out on Intel® Core™ i7-7820HQ CPU up to 3.90 GHz microprocessor and 16Gb RAM.

### 2.4. Glucose Induced Insulin Secretion Test (GIIST)

In vitro functionality of MIN6 aggregates was evaluated by Glucose Induced Insulin Secretion Test (GIIST) in the transwell membrane system placed in the custom-made experimental setup illustrated in Fig. 2. Modified Krebs buffer (115 mM NaCl, 5 mM KCl, 24 mM NaHCO$_3$, Sigma) supplemented with 2.2 mM CaCl$_2$, 20 mM HEPES (Gibco), 30% bovine serum albumin, 1 mM MgCl$_2$, and 0.1 mM Theophylline (Sigma) was prepared at pH 7.4 and used to prepare low (1.67 mM) and high (16.7 mM) glucose concentration solutions.

GIIST protocol includes the following steps: (1) pre-incubation of 90 min in buffer; (2) incubation in subsequent LGC (60 min)/HGC (60 min); (3) three times 5 min washing in the buffer (4) steps 2 and 3 are cycled. During GIIST steps, both top and bottom compartments were supplemented with 300 μL of medium at the same glucose concentration.

## 3. Results

Section 3 includes: (i) simulated and experimental results for insulin secretion in MIN6 aggregates cultured in open system, whose fitting allowed at optimizing the model parameters (Section 3.1); (ii) simulated and experimental GIIST results on MIN6 aggregates cultured in open system, to validate the ability of the model in predicting the dynamical response of the membrane-based encapsulation device under cycled LGC and HGC stimuli (Section 3.2) ; (iii) simulated and experimental GIIST results on human pancreatic islets cultured in closed system, including comprehensive modelling of oxygen and glucose profiles within the device (Section 3.3); (iv) application of the model to geometry optimization of microwell membrane system cultured with human islets (Section 3.4).

### 3.1. Insulin secretion and diffusion

Fig. 3 shows the insulin secretion over 60 min when MIN6 aggregates, cultured in the open system, are exposed to high glucose concentration (16.7 mM) only in the bottom compartment (see Fig. 2). Glucose solution was prepared from modified Krebs buffer whose composition is described in Section 2.4. Model prediction confirms that diffusing glucose induces a rapid production of insulin within the first ten minutes (the experimental concentration of 50.5 μg/L reached in the top compartment is underestimated by the mathematical model by 24%). Data are coherent with a linear insulin secretion rate characterizing Phase I. The trend of the modeled insulin concentration curve is in good agreement with the measured data, showing a peak at about 10 min with production rate of $1 \times 10^{-22}$ mol/(cell s), followed by a decrement and succes-

**Table 1 – Parameter values used as input to the FEM model.**

| Location | Parameter | Value | Description | Ref. |
|---|---|---|---|---|
| Culture medium | $c_{O_2}^0$ | $2 \times 10^{-7}$ mol cm$^{-3}$ | Initial oxygen concentration[a] | This work |
| | $c_G^0$ | $1.67 \times 10^{-6}$ mol cm$^{-3}$ | Low Glucose Concentration (LGC) | |
| | | $1.67 \times 10^{-5}$ mol cm$^{-3}$ | High Glucose Concentration (HGC) | |
| | $c_I^0$ | 0 mol cm$^{-3}$ | Initial insulin concentration | |
| | $D_{O_2}^m$ | $3 \times 10^{-5}$ cm$^2$ s$^{-1}$ | Oxygen diffusion coefficient | Dulong and Legallais (2005) |
| | $D_G^m$ | $9 \times 10^{-6}$ cm$^2$ s$^{-1}$ | Glucose diffusion coefficient | Tziampazis and Sambanis (1995) |
| Trans-well membrane, lid | $D_I^m$ | $1.5 \times 10^{-6}$ cm$^2$ s$^{-1}$ | Insulin diffusion coefficient | |
| | $D_{O_2}^s$ | $3 \times 10^{-6}$ cm$^2$ s$^{-1}$ | Oxygen diffusion coefficient | Papenburg et al. (2011) |
| | $D_G^s$ | $1 \times 10^{-6}$ cm$^2$ s$^{-1}$ | Glucose diffusion coefficient | Skrzypek et al. (2017) |
| | $D_I^s$ | $3 \times 10^{-7}$ cm$^2$ s$^{-1}$ | Insulin diffusion coefficient | |
| | $D_{O_2}^i$ | $2 \times 10^{-5}$ cm$^2$ s$^{-1}$ | Oxygen diffusion coefficient | Buckwald (2011) |
| | $D_G^i$ | $3.8 \times 10^{-7}$ cm$^2$ s$^{-1}$ | Glucose diffusion coefficient | Kauri et al. (2003) |
| | $D_I^i$ | $5 \times 10^{-7}$ cm$^2$ s$^{-1}$ | Insulin diffusion coefficient | Buladi et al. (1996) |
| | $r_{O_2}$ | $-3.75 \times 10^{-17}$ mol cell$^{-1}$ s$^{-1}$ | Zero-order oxygen uptake rate | Ye et al. (2006) |
| | $r_G$ | $-\phi \cdot 3.8 \times 10^{-16}$ mol cell$^{-1}$ s$^{-1}$ | | Ye et al. (2006), Wang et al. (2005) |
| | | $\phi = 1$ for MIN6 | Zero-order glucose uptake rate[b] | |
| | | $\phi = 1$ for Human at LGC | | |
| | | $\phi = 2$ for Human at HGC | | |
| Pancreatic islets | $t_1^*$ | 240 s | | |
| | $t_2^*$ | 300 s | | |
| | $\alpha_1$ | $1.9 \times 10^{-2}$ s$^{-1}$ | | |
| | $\alpha_2$ | $6.5 \times 10^{-4}$ s$^{-1}$ | | |
| | $\beta$ | $\psi \cdot 3.5 \times 10^{-15}$ mol cm$^{-3}$ s$^{-2}$ | | |
| | | $\psi = 1$ for MIN6 | | |
| | | $\psi = 0.1$ for Human | | This work |
| | $V_{m,1}$ | $\psi \cdot 5.33 \times 10^{-13}$ mol cm$^{-3}$ s$^{-1}$ | Kinetic parameters for insulin production rate | |
| | | $\psi = 1$ for MIN6 | | |
| | | $\psi = 0.1$ for Human | | |
| | $V_{m,2}$ | $\psi \cdot 3.25 \times 10^{-14}$ mol cm$^{-3}$ s$^{-1}$ | | |
| | | $\psi = 1$ for MIN6 | | |
| | | $\psi = 0.2$ for Human | | |
| | $K_{m,1}$ | $6.4 \times 10^{-7}$ mol cm$^{-3}$ | | |
| | $K_{m,2}$ | $3.1 \times 10^{-7}$ mol cm$^{-3}$ | | |
| | $c_{G,1}$ | $1.5 \times 10^{-7}$ mol cm$^{-3}$ | | Thrash (2010) |
| | $c_{G,2}$ | $8.6 \times 10^{-8}$ mol cm$^{-3}$ | | |

[a] In equilibrium with 20% $O_2$ partial pressure.
[b] $\phi$: glucose uptake enhancement factor; LGC: Low Glucose Concentration; HGC: High Glucose Concentration.
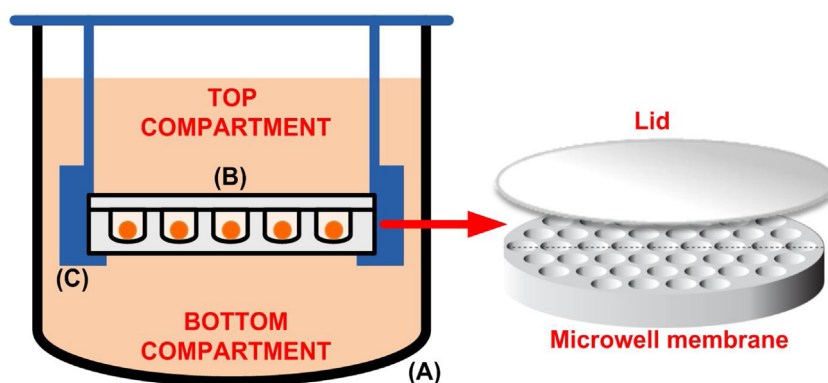


**Fig. 2 – Experimental setup. (A) well plate; (B) transwell membrane system (here illustrated with lid) containing islets; (C) sealing ring adapted from Skrzypek et al., 2017.**

sive increase (at about 30 min). Due to diffusional hindrance, the insulin concentration in the bottom compartment is lower than in the top compartment, reaching a concentration of 41.6 µg/L after one hour.

The insulin release on the top compartment (Fig. 3a) is consistent to the *in vitro* biphasic behavior of insulin production under application of high glucose concentration: glucose elicit induces insulin release through an adenosine triphosphate-sensitive K$^+$ channel (K$_{ATP}$ channel)-dependent mechanism, which is gradually augmented in a K$_{ATP}$ channel-independent

manner (Komatsu et al., 2013). The authors investigated there the effect of ACTH stimulation on insulin secretion and reported that MIN6 pseudo-islets perfused with buffer containing 2 mM glucose produced insulin with the rate of 0.589 ng/30,000 cells/h (i.e. $\sim 9 \times 10^{-22}$ mol/cell s). Increasing the glucose content of the medium to 8 mM (stimulation protracted for 20 min) caused a rapid and marked increase in insulin secretion with a typical, transient first phase peak (249 ± 15%) followed by a sustained second phase of secretion
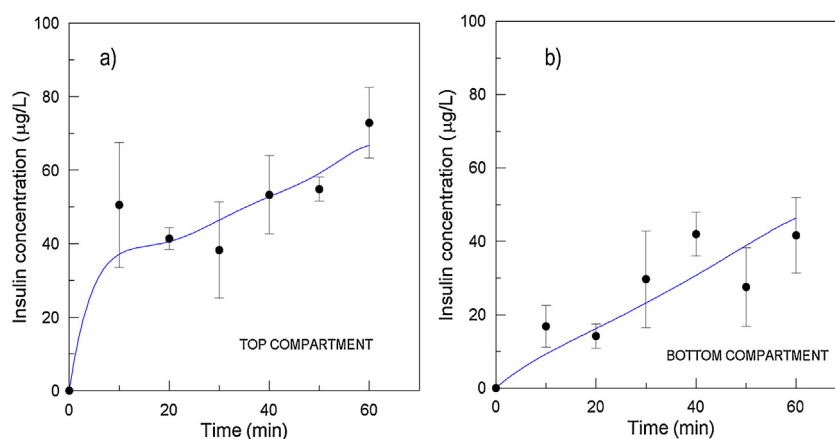
**Fig. 3 – Time-variant simulated and experimental insulin concentration secreted by MIN6 aggregates in (a) top compartment; (b) bottom compartment. Insulin is secreted as a response to high glucose concentration (HGC: 16.7 mM) in the bottom compartment. Symbol: experimental data, line: modeling results. Open system configuration. Membrane thickness: 250 μm. Data obtained from Skrzypek et al., (2017).**

(Al-Majed et al., 2004), consistent to the release observed in our study.

### 3.2. GIIST on MIN6 aggregates in open system

Fig. 4 compares the transient simulation output and experimental data for the open system (membrane thickness of 250 μm) subjected to a Glucose Induced Insulin Secretion Test as described in Section 2.4. Specifically, data refers to insulin concentration simulated/measured first after 60 min exposure to Low Glucose Concentration (preceded by 90 min pre-incubation in buffer), then after 60 min exposure to High Glucose Concentration, then again after 60 min exposure to Low Glucose Concentration (preceded by washing in buffer).

A good agreement between theoretical and measured insulin concentration values in the top compartment is observed.

Overall, the increase in glucose concentration from 1.67 mM to 16.7 mM causes an increase of 140% c.a. in insulin concentration. In general, the difference between predicted and experimental values of insulin concentration in the bottom compartment spans from 20% in HGC to 15% c.a. in LGC.

Llanos et al. (2015) observed that stimulatory glucose test (from 2.8 mM to 16.7 mM) carried out on rat pancreatic islets increased the insulin secretion rate from an average basal value of 4.7–12.6 μg/(L h) (Llanos et al., 2015). This value is in close agreement with the insulin concentration value modeled here for HGC step, which is $14.6 \pm 6.5$ μg/(L) in the first cycle.

The model also predicts very well the insulin delivery of an open system with lower thickness of 100 μm. Fig. 5 compares the related concentration profiles of secreted insulin during a GIIST for both LGC and HGC steps. On one hand, the highest insulin concentration is reached at the center of the islet, i.e. 9.4 μg/L and 21.5 μg/L under LGC and HGC, respectively. Due to the non-hindered diffusion through the culture medium, insulin concentration is almost uniform within the wells (LGC: 8.5 μg/L, HCG: 20.7 μg/L). On the other hand, diffusion of insulin to the bottom compartment is lower due the membrane, leading to the minimum insulin concentration at the interface: here, the value of insulin concentration is reduced by 16% and 7% for LGC and HGC steps, respectively. These results reflect the difference in the average diffusive

flux within the polymeric membrane ($\sim$0.25 mol/cm$^2$ s) with respect to the one computed in the well ($\sim$0.6 mol/cm$^2$ s).

### 3.3. GIIST on Human pancreatic islets in closed system

Encapsulation of pancreatic islets in a closed microwell membrane system might eventually pose problems in terms of sufficient oxygen availability. Human pancreatic islets possess a widespread intra-islet vasculature needed to efficiently transfer oxygen and nutrients and metabolic wastes, receiving around 10–20% of the total blood flow of the pancreas (Komatsu et al., 2013). Conversely, the viability and function of non-vascularized encapsulated pancreatic islets with significant metabolic demand is often limited by hypoxia, during culture or immediately following transplantation, as a result of non-adequate oxygen supply under concentration gradient-driven diffusion.

Although oxygen is consumed at approximately the same rate as glucose and exhibits about three times higher diffusion coefficient in water, it has low solubility in aqueous media (0.2 mM vs. 5–10 mM) and, therefore, its supply to the cells can be a critical factor for successful implementation of the encapsulation device. Fig. 6a shows that oxygen concentration profile in the device is higher than the critical value of 40 mmHg, i.e. the partial pressure of $O_2$ in the venous blood corresponding to a concentration of $5 \times 10^{-5}$ mol/L (Sumaru and Kanamori, 2004) and assumed as threshold for full viability and functionality of cells (Colton, 2014). This is also facilitated by the relatively low cell surface coverage (about 170 islets/cm$^2$). The modeled $O_2$ concentration profile appears parabolic within the cultured islets (assumed as spherical) and almost linear in the other parts of the transwell membrane system. The minimum oxygen concentration ($1.5 \times 10^{-4}$ mol/L) reached at the center of cultured islets exposed to high glucose stimulus, is lower by 14% with respect to the corresponding value for LGC. This is consistent to previous findings of Wang et al. (2005) who, using an accurate oxygen biosensor system, observed that significant increase in oxygen consumption rate (OCR) was attained for human islets exposed to high glucose concentration (16.7 or 33.3 mM) with respect to basal value (5.6 mM); for 200 IE (islet equivalents) of human islets in 200 μL CMRL 1066 culture medium, OCR practically doubled from $\sim$2.5 × 10$^{-4}$ to $\sim$5 × 10$^{-4}$ fmol/min/100IE. Since the oxygen gradient is mainly
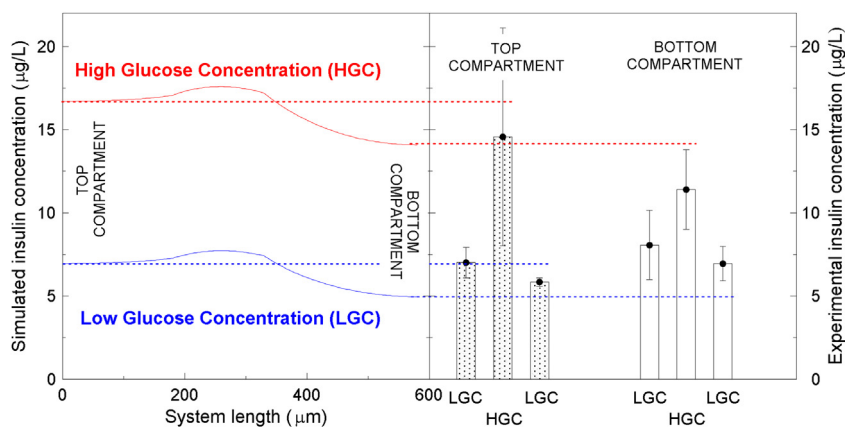
Fig. 4 – Left side: simulated insulin concentration secreted by MIN6 aggregates in top and bottom compartments as a response to LGC (1.67 mM) and HGC (16.7 mM). Right side: experimental insulin concentration measured in top and bottom compartments as response to LGC/HGC/LGC changes. Data obtained from Skrzypek et al., (2017). Open system configuration. Membrane thickness: 250 μm.
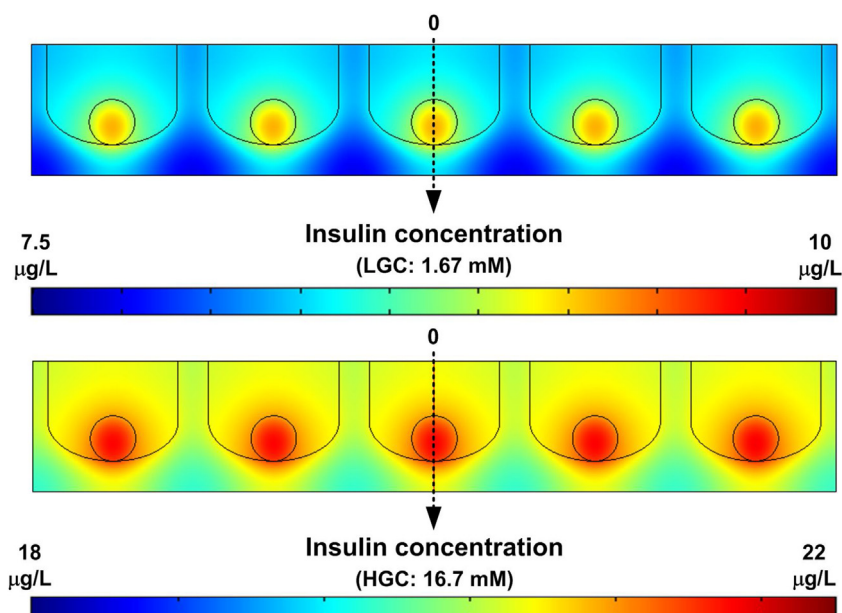


Fig. 5 – Modeled profiles of insulin concentration within the microwell membrane system as a result of GIIST under low (1.67 mM) and high (16.7 mM) glucose concentration solutions. Membrane thickness: 100 μm.

developed inside the islet structure, an appropriate optimization of cellular aggregate size and density, device geometry and membrane properties are required to supply an adequate oxygen amount to maintain isolated islets viable, as confirmed in other studies (Komatsu et al., 2017; McReynolds et al., 2017). In later section of this study, we also present the application of the developed model for designing an optimized microwell device with optimal geometry and suitable for hosting smaller size islets.

Fig. 6b presents the glucose concentration profile of the closed system. In the presence of high glucose stimulation (HGC step), the concentration decreases from the islet surface to the center for about 7%. Kauri et al. (2003) measured an analogous glucose concentration decrease in the center of cultured islets (10–20%) for islets with a diameter of 180–220 μm. In general, unlike oxygen, the glucose transport is often not a limiting factor since – under physiological conditions – its concentration (3−15 mM) is generally two orders of magnitude higher than $O_2$ (Martin and Vermette, 2005). The response of human islets to glucose square-wave stimulation is illustrated in Fig. 6c. Comparison between simulation and experimental

results was done on the top of the device, since the presence of the lid mitigates the difference of insulin concentration between top and bottom compartments. Interestingly, the predicted increase in insulin production for the human islets when shifting from LGC to HGC (~190%) is higher than the one observed for the MIN6 aggregates (~140%).

### 3.4. Closed system optimization using the developed model

In the earlier sections, we showed that the developed model predicts accurately the performance of the current microwell device. In this section, the developed model is applied for designing an improved microwell membrane; in fact, the delivery of insulin is predicted for devices having geometry characterized by small microwell width and depth, as well as, smaller spacing between the wells. Smaller wells are desired for: (i) improving the delivery of oxygen and nutrients to the encapsulated cells, (ii) having high transport of glucose into the device and (iii) higher insulin delivery by the cells. Smaller size of microwells and smaller spacing between the wells will
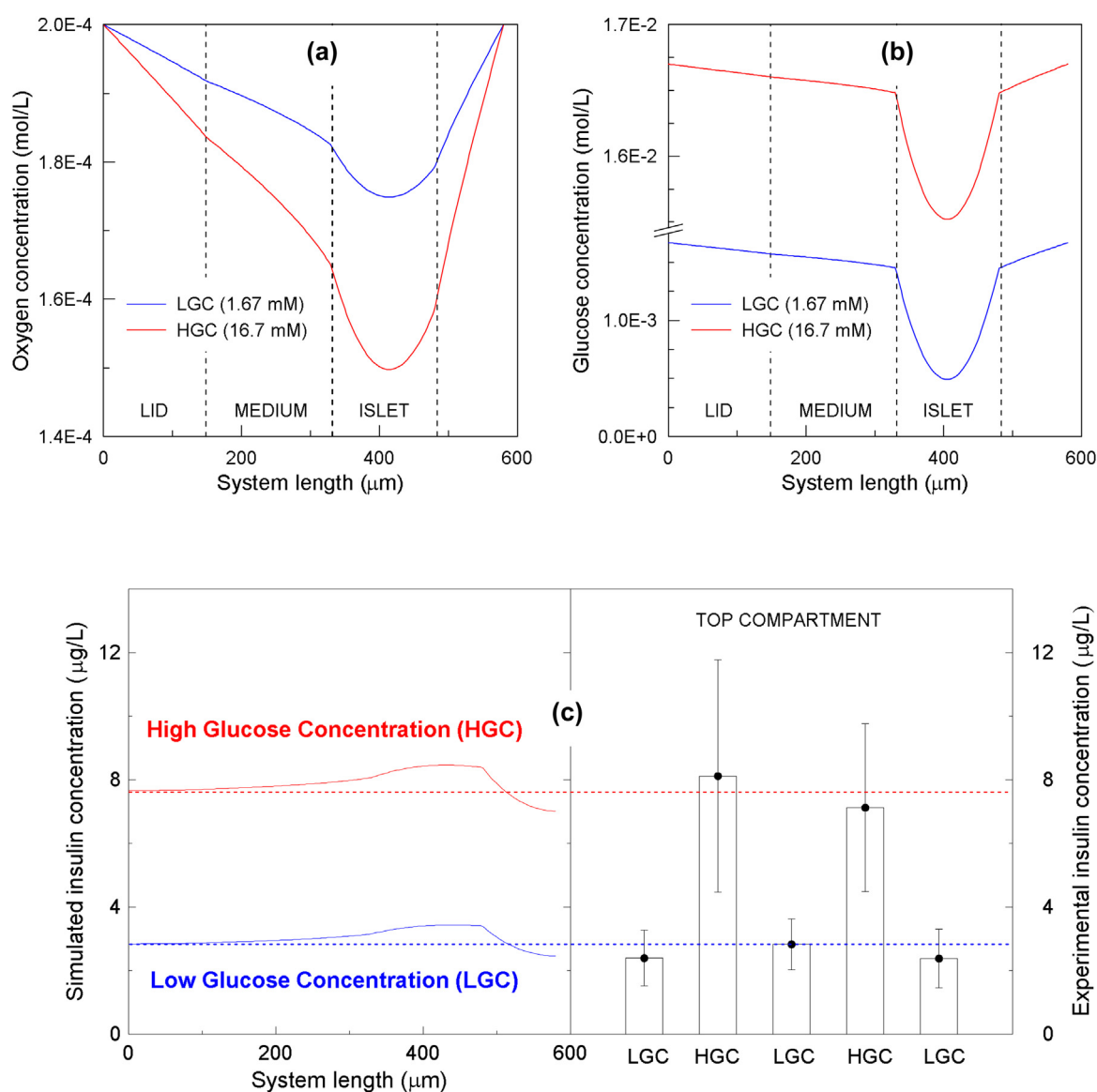
**Fig. 6 – Simulated concentration profiles within the transwell membrane system cultured with human islets and covered with the lid under LGC and HGC. (a) oxygen; (b) glucose; (c) left side: insulin; right side: experimental insulin concentration measured in as response to cycled LGC/HGC hourly step changes. Membrane thickness: 100 μm. Data obtained from Skrzypek et al., (2017).**

achieve high islet encapsulation density (higher number of islets encapsulated per surface area of the device) facilitating the upscaling of the device and its implementation in the clinic.

Fig. 7 summarizes the device characteristics modelled and the obtained results concerning insulin delivery. For the microwell spacing we did not model spacing lower than 10 μm or device thickness lower than 50 μm, since we anticipate that such devices will be challenging to manufacture reproducibly. Concerning the microwell width and depth, the thresholds on modelled size are related to the possibility to accommodate a single islet with diameter of 150 μm (Fig. 7a). In general, our results show that the reduction of device dimensions decreases the resistance to mass transport and, hence, enhances the concentration of insulin on the top and bottom of the closed microwell device. Moreover, the difference in delivery of insulin between top and bottom of the closed device is less than 10%.

With respect to the benchmark model illustrated in Fig. 1e (namely Case Study 1 in Fig. 7a), a reduction of vertical dimen-

sions (Case Study 2), i.e ∼40% in microwell depth (parameter "b" from 330 to 200 μm) and 50% in membrane thickness (parameter "d" from 100 to 50 μm), results in an increase of insulin concentration on the top compartment under LGC and HGC of 121% and 72%, respectively. Moreover, a reduction of horizontal dimensions (Case Study 3), i.e ∼58% in microwell width (parameter "a" from 430 to 180 μm) and 90% in microwell spacing (parameter "c" from 100 to 10 μm), results in an increase of insulin concentration on the top of the device under LGC and HGC of 145% and 164%, respectively.

Time-variant predicted insulin response to stepwise increments in the incoming glucose content (from LGC to HGC) are illustrated in Fig. 7b for both top and bottom positions of the microwell device. The biphasic behavior of insulin release by the islets appears again clearly in a quick first phase consisting of a transient spike (duration of about 500–600 s) followed by a second phase characterized by a slower secretion rate.

We define an Insulin Secretion Efficiency ($\varepsilon_{I/10}$) as the ratio between the actual average insulin secretion rate ($\bar{r}_I$) and the insulin secretion rate in absence of mass transfer limitations
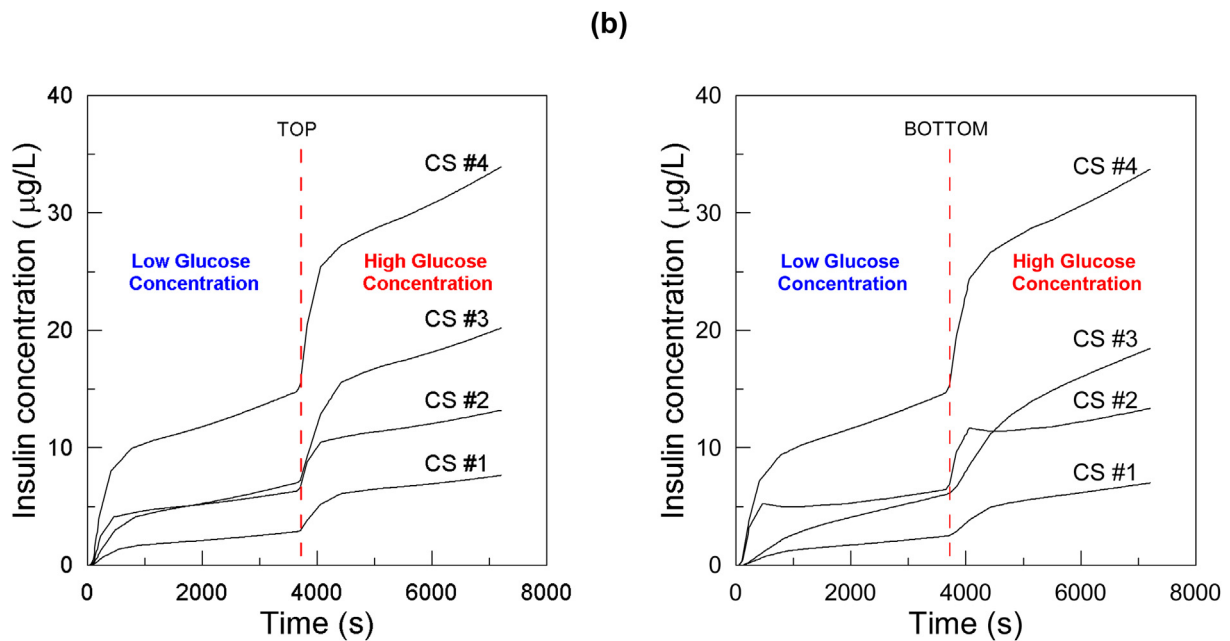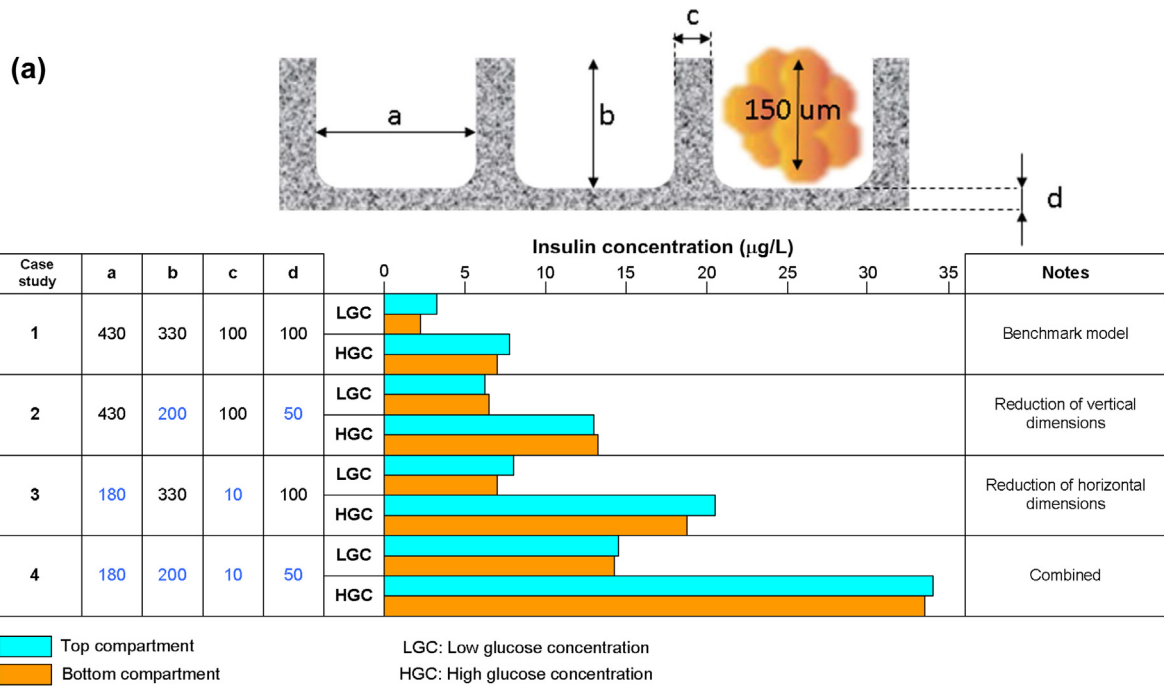
Fig. 7 – Summary of optimization results as a function of geometrical characteristics of microwell membrane system cultured with human islets under LGC and HGC: (a) Total insulin concentration on the top and bottom of the device; (b) Simulated time-variant insulin concentration profiles on the top and bottom of the microwell systems (Case Studies 1–4).

$(r_{I, max})$, i.e. with cells exposed to glucose concentration set in the top compartment:

$$\varepsilon_{I/600} = \frac{\bar{r}_I}{r_{I, max}} \tag{4}$$

where both rates evaluated after 600 s having considered that insulin concentration profiles develop predominantly within the first minutes of secretion activity.

Results show that $\varepsilon_{I/10}$ approaches unity when microwells are exposed to High Glucose Concentration, for all case studies investigated. On the other hand, under LGC, the efficiency

span from the highest value of 0.78 for CS#4, to the lowest value of 0.68 for CS#1.

According to Eqs. (2.b)–(2.d), the Phase II insulin secretion rate is enhanced at higher glucose concentration; therefore, an improvement of mass transfer in Case Studies 3 and 4 results in a more sustained production of insulin. Moreover, insulin concentration profiles exhibit similar slopes (at LGC: $1.8 \times 10^{-3}$ μg/L s for CS#4, $1.1 \times 10^{-3}$ μg/L s for CS#3; at HGC: $2.1 \times 10^{-3}$ μg/L s for CS#4, $1.7 \times 10^{-3}$ μg/L s for CS#3), almost double with respect to those predicted for CS#2 and CS#1.

Our modelling results show that the device with the optimal performance in terms of insulin secretion (significant increments of about 420% and 340% on the top of the device
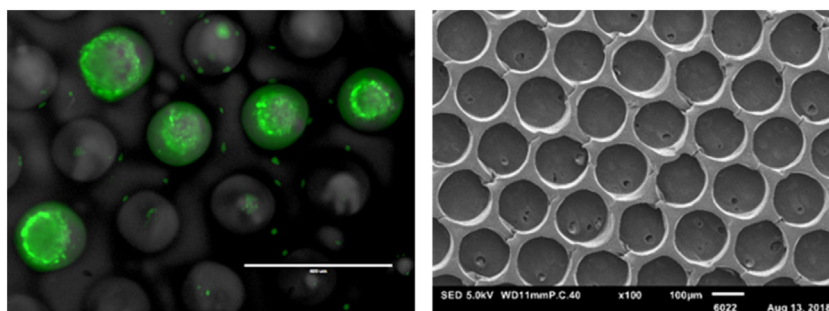
Fig. 8 – Preliminary microwell membrane optimization study: (a) PES/PVP microwell membrane with microwell dimeter: 180 μm, microwell depth: 200 μm, microwell spacing: 10 μm, and membrane thickness: 50 μm; (b) viability of MIN6 aggregates after 1 day of culture within optimized microwell membrane (0.25 μL/mL calcein (green, live) and 3 μL/mL ethidium homodimer (red, dead) in PBS staining for 30 min at 37 °C). (For interpretation of the references to color in this figure legend, the reader is referred to the web version of this article.)

under LGC and HGC, respectively) is that of Case Study 4: microwell width: 180 μm, microwell depth: 200 μm, microwell spacing: 10 μm, and membrane thickness: 50 μm. Following these modelling results we have actually performed preliminary studies of fabricating an optimized microwell membrane device using PSμM onto a dedicated mold as well as performed preliminary human islets culture studies, see Fig. 8. These first results are very promising, the reproduction of porous microwells is very good and each microwell can accommodate one islet. In the future, we plan to perform optimization of the cell seeding and detailed investigation of the device function *in vitro* and *in vivo*. Assuming maximum loading with islets in such device, we would need 2 microwell membranes of 10 cm diameter each for treating a patient of 70 kg (total encapsulation of 350,000 islets = 70 kg × 5000 islets/kg) which is feasible.

## 4. Conclusions

In this work, firstly we have developed and validated a computational model for the function of a membrane based macroencapsulation device of pancreatic islets, providing a detailed spatial-temporal description of concentration profiles of oxygen, glucose and insulin. The results showed that the microwell system could provide adequate supply of necessary nutrients (with particular focus on oxygen, the primary limiting factor in the survival of cells cultured in poorly- or non-vascularized environment due to its low solubility in aqueous media) and appropriate and timely release of insulin by encapsulated islets. The glucose-induced insulin secretion kinetics, coupled with the diffusive transport of species, allowed to predict with sufficient accuracy the dynamic response under square-wave glucose stimulus in the device, consistent to a biphasic pattern composed by an initial release developing rapidly but lasting only a few minutes (first phase), followed by a secretion sustained in time (second phase).

Subsequently, the developed computational model was applied for the design and optimization of the geometry of the device for 150 μm human islets culture. The optimized device with microwell width of 180 μm, microwell depth of 200 μm, microwell spacing of 10 μm, and membrane thickness of 50 μm, was also manufactured quite reproducibly and first tests of cell culture were very promising. In the future, detailed *in vitro* and *in vivo* investigation of the optimized device will be performed.

## Conflict of interest

The authors declare that there are no conflicts of interest.

## Author contributions

K.S. performed literature search, experimental design, data collection, data analysis, data interpretation and manuscript writing. E.C. performed the modeling studies and contributed to experimental design, data analysis data interpretation and manuscript writing. D.S. contributed to experimental design, data interpretation and manuscript writing.

## Acknowledgments

## Appendix A. Supplementary data

Supplementary data associated with this article can be found, in the online version, at https://doi.org/10.1016/j.cherd.2019.11.020.

## References

Al-Majed, H.T., Jones, P.M., Persaud, S.J., Sugden, D., Huang, G.C., Amiel, S., Whitehouse, B.J., 2004. ACTH stimulates insulin secretion from MIN6 cells and primary mouse and human islets of Langerhans. J. Endocrinol. 180, 155–166.

Borg, D.J., Bonifacio, E., 2011. The use of biomaterials in islet transplantation. Curr. Diab. Rep. 11 (58), 434–444.

Buchwald, P., Wang, X., Khan, A., Bernal, A., Fraker, C., Inverardi, L., Ricordi, C., 2009. Quantitative assessment of islet cell products: estimating the accuracy of the existing protocol and accounting for islet size distribution. Cell Transplant. 18, 1223–1235.

Buckwald, P., 2011. A local glucose- and oxygen concentration-based insulin secretion model for pancreatic islets. Theor. Biol. Med. Model. 8 (20), 1–25.

Buladi, B.M., Chang, C.C., Belovich, J.M., Gatica, J.E., 1996. Transport phenomena and kinetics in an extravascular bioartificial pancreas. AIChE J. 42, 2668–2682.

Chun, S., Huang, Y., Xie, W.J., Hou, Y., Huang, R.P., Song, Y.M., Liu, X.M., Zheng, W., Shi, Y., Song, C.F., 2008. Adhesive growth of pancreatic islet cells on a polyglycolic acid fibrous scaffold. Transplant. Proc. 40 (5), 1658–1663.

Colton, C.K., 2014. Oxygen supply to encapsulated therapeutic cells. Adv. Drug Deliv. Rev. 67 (68), 93–110.

Curcio, E., Piscioneri, A., Salerno, S., Tasselli, F., Morelli, S., Drioli, E., De Bartolo, L., 2012. Human lymphocytes cultured in 3-D bioreactors: influence of configuration on metabolite transport and reactions. Biomaterials 33 (2012), 8296–8303.

Curcio, E., Piscioneri, A., Morelli, S., Salerno, S., Macchiarini, P., De Bartolo, L., 2014. Kinetics of oxygen uptake by cells potentially used in a tissue engineered trachea. Biomaterials 35 (25), 6829–6837.

Daly, M.E., Vale, C., Walker, M., Littlefield, A., Alberti, K.G., Mathers, J.C., 1998. Acute effects on insulin sensitivity and diurnal metabolic profiles of a high-sucrose compared with a high-starch diet. Am. J. Clin. Nutr. 67 (6), 1186–1196.

de Vos, P., Lazarjani, H.A., Poncelet, D., Faas, M.M., 2014. Polymers in cell encapsulation from an enveloped cell perspective. Adv. Drug Deliv. Rev. 67 (68), 15–34.

Dulong, J.-L., Legallais, C., 2005. What are the relevant parameters for the geometrical optimization of an implantable bioartificial pancreas? J. Biomech. Eng. 127, 1054–1061.

Emamaullee, J.A., Shapiro, A.M., 2006. Interventional strategies to prevent beta-cell apoptosis in islet transplantation. Diabetes 55 (7), 1907–1914.

Groot Nibbelink, M., Skrzypek, K., Karbaat, L., Both, S., Plass, J., Klomphaar, B., van Lente, J., Henke, S., Karperien, M., Stamatialis, D., van Apeldoorn, A., 2018. An important step towards a prevascularized islet microencapsulation device — in vivo prevascularization by combination of mesenchymal stem cells on micropatterned membranes. J. Mater. Sci.: Mater. Med. 29 (11), 174.

Kauri, L.M., Jung, S.K., Kennedy, R.T., 2003. Direct measurement of glucose gradients and mass transport within islets of Langerhans. Biochem. Biophys. Res. Commun. 304, 371–377.

Komatsu, M., Takei, M., Ishii, H., Sato, Y., 2013. Glucose-stimulated insulin secretion: a newer perspective. J. Diabetes Investig. 4 (6), 511–516.

Komatsu, H., Cook, C., Wang, C.-H., Medrano, L., Lin, H., Kandeel, F., Tai, Y.-C., Mullen, Y., 2017. Oxygen environment and islet size are the primary limiting factors of isolated pancreatic islet survival. PLoS One 2 (8), 1–17, http://dx.doi.org/10.1371/journal.pone.0183780.

Liao, S.W., Rawson, J., Omori, K., Ishiyama, K., Mozhdehi, D., Oancea, A., Ito, T., Guan, Z., Mullen, Y., 2013. Maintaining functional islets through encapsulation in an injectable saccharide-peptide hydrogel. Biomaterials 34 (16), 3984–3991.

Lien, C.-C., Chen, P.-J., Venault, A., Tang, S.-H., Fu, Y., Dizon, G.V., Aimar, P., Chang, Y., 2019. A zwitterionic interpenetrating network for improving the blood compatibility of polypropylene membranes applied to leukodepletion. J. Membr. Sci. 584, 148–160.

Llanos, P., Contreras-Ferrat, A., Barrientos, G., Valencia, M., Mears, D., Hidalgo, C., 2015. Glucose-dependent insulin secretion in pancreatic β-cell islets from male rats requires Ca²⁺ release via ROS-Stimulated ryanodine receptors. PLoS One 10 (6), e0129238.

Martin, Y., Vermette, P., 2005. Bioreactors for tissue mass culture: design, characterization, and recent advances. Biomaterials 26, 7481–7503.McReynolds, J., Wen, Y., Li, X., Guan, J., Jin, S., 2017. Modeling spatial distribution of oxygen in 3D culture of islet beta-cells. Biotechnol. Prog. 33 (1), 221–228.

Papenburg, B.J., Vogelaar, L., Bolhuis-Versteeg, L.A.M., Lammertink, R.G.H., Stamatialis, D., Wessling, M., 2007. One-step fabrication of porous micropatterned scaffolds to control cell behavior. Biomaterials 28, 1998–2009.

Papenburg, B.J., Higuera, G.A., de Vries, I.-J., de Boer, J., van Blitterswijk, C.A., Wessling, M., Stamatialis, D., 2011. Model to design multilayer tissue engineering scaffolds. Macromol. Symp. 309 (310), 84–92.

Rivron, N.C., Vrij, E.J., Rouwkema, J., Le Gac, S., van den Berg, A., Truckenmüller, R.K., van Blitterswijk, C.A., 2012. Tissue deformation spatially modulates VEGF signaling and angiogenesis. Proc. Natl. Acad. Sci. U. S. A. 109, 6886–6891.

Shapiro, A.M.J., Pokrywczynska, M., Ricordi, C., 2017. Clinical pancreatic islet transplantation. Nat. Rev. Endocrinol. 13, 268–277.

Skrzypek, K., Groot Nibbelink, M., van Lente, J., Buitinga, M., Engelse, M.A., de Koning, E.J.P., Karperien, M., van Apeldoorn, A., Stamatialis, D., 2017. Pancreatic islet macroencapsulation using microwell porous membranes. Sci. Rep. 7, 9186.

Skrzypek, K., Brito Barrera, Y., Groth, T., Stamatialis, D., 2018a. Endothelial and beta cell composite aggregates for improved function of a bioartificial pancreas encapsulation device. Int. J. Artif. Organs 41 (3), 152–159.

Skrzypek, K., Groot Nibbelink, M., Karbaat, L.P., Karperien, M., van Apeldoorn, A., Stamatialis, D., 2018b. An important step towards a prevascularized islet macroencapsulation device — effect of micropatterned membranes on development of endothelial cell network. J. Mater. Sci.: Mater. Med. 29 (7), 91.

Strand, B.L., Coron, A.E., Skjak-Braek, G., 2017. Current and future perspectives on alginate encapsulated pancreatic islet. Stem Cells Transl. Med. 6, 1053–1058.

Sumaru, K., Kanamori, T., 2004. Optimal design of bio-hybrid systems with a hollow fiber scaffold: model analysis of oxygen diffusion/consumption. Biochem. Eng. J. 20, 127–136.

Thrash, M., 2010. Modeling oxygen transport in a cylindrical bioartificial pancreas. ASAIO J., 338–343.

Tziampazis, E., Sambanis, A., 1995. Tissue engineering of a bioartificial pancreas: modeling the cell environment and device function. Biotechnol. Prog. 11, 115–126.

Wang, W., Upshaw, L., Strong, D.M., Robertson, R.P., Reems, J., 2005. Increased oxygen consumption rates in response to high glucose detected by a novel oxygen biosensor system in non-human primate and human islets. J. Endocrinol. 185, 445–455.

Ye, H., Das, D.B., Triffitt, J.T., Cui, Z.F., 2006. Modelling nutrient transport in hollow fibre membrane bioreactors for growing three-dimensional bone tissue. J. Membr. Sci. 272, 169–178.